PCCP

PAPER

View Article Online
View Journal | View Issue

Cite this: *Phys. Chem. Chem. Phys.*, 2024, **26**, 3907

Breaking the Hoff/Le Bel rule by an electron-compensation strategy: the global energy minimum of $NGa_4S_4^+$†

Xiu-dong Jia *[a] and Zhi-wei Du[b]

Received 31st October 2023,
Accepted 2nd January 2024

DOI: 10.1039/d3cp05290g

rsc.li/pccp

In tetracoordinate chemistry, there is an attractive scientific problem of how to make the planar configuration more stable than the tetrahedral configuration. For tetracoordinate nitrogen, the abundant studies indicate that the planar tetracoordinate nitrogen (ptN) is far less stable than the tetrahedral tetracoordinate nitrogen (ttN). Herein, we introduced four S atoms to the unstable ptN-NGa_4^+ and stable ttN-NGa_4^+ by following an electron-compensation strategy. Surprisingly, ptN-$NGa_4S_4^+$ is more stable than ttN-$NGa_4S_4^+$. Thermodynamically, ptN-$NGa_4S_4^+$ is the global energy minimum, which is 46.7 kcal mol^{-1} lower in energy than ttN-$NGa_4S_4^+$. Dynamically, the BOMD simulations indicated that ptN-$NGa_4S_4^+$ has excellent dynamic stability at 4, 298, 500 and 1000 K, but the ttN-$NGa_4S_4^+$ is isomerized at 1000 K. Electronically, the HOMO–LUMO gap of ptN-$NGa_4S_4^+$ (6.91 eV) is much wider than that of ttN-$NGa_4S_4^+$ (5.25 eV). Moreover, AdNDP analyses showed that the eight 2c–2e Ga–S σ-bonds eliminated the $4s^2$ lone pair/$4s^2$ lone pair repulsion between the four Ga atoms and provided a strong spatial protection for ptN-$NGa_4S_4^+$; and that the four 3c–2e Ga-S-Ga π back-bonds could compensate electrons for Ga, weakening the electron-deficiency of Ga. Simultaneously, the double 6σ/2π aromaticity further enhanced the stability of ptN-$NGa_4S_4^+$. Thus, as the dynamically stable global energy minimum displaying double aromaticity, ptN-$NGa_4S_4^+$ will be more promising than ttN-$NGa_4S_4^+$ in gas phase generation.

Introduction

The investigation of planar hypercoordinate carbon (phC) chemistry has enriched the chemical bonding theory and promoted the development of the non-classical molecules.[1] In 1970, Hoffmann *et al.* first proposed planar tetracoordinated carbon (ptC),[2] which violates the basic Hoff/Le Bel rule[3,4] (tetrahedral tetracoordinate carbon, ttC) in organic stereochemistry. After nearly 50 years of vigorous development, the study on phC has made many significant advances, including the observed CAl_4^-,[5] CAl_4^{2-},[6] CAl_3Si^-, CAl_3Ge^-,[7] C_2Al_4,[8] and $C_5Al_5^-$,[9] as well as a series of computationally verified global energy minima with a planar pentacoordinate[10] or hexacoordinate carbon.[11] Even so, the abundant experimental and theoretical studies have found that ptC and ttC have been in competition and the latter is more stable in most cases. Taking CH_4 as an example, methane is required to cross a large energy barrier of 130 kcal mol^{-1} to isomerize into planar methane, even 27 kcal mol^{-1} higher than the dissociation energy (103 kcal mol^{-1}) of the C–H bond in methane.[12] Another example is CM_4 (M = B, Al, Ga, In and Tl), which generally prefers the comfortable ttC configuration due to the lone pair/lone pair repulsion of M ns^2 electrons. Furthermore, the strong electron deficiency of M has made the electronic structure of the ptC-CM_4 more unstable.[6] Therefore, in ptC chemistry, there is an important scientific problem of how to reduce the stability of ttC while increasing the stability of ptC.

To solve this problem, many theorists have contributed, among whom Wu *et al.* put forward a valid electron-compensation strategy in 2022 and successfully designed ptC species CB_8O_8.[13] As shown in Scheme 1, the electronegative atom X (such as N, O, S, *etc.*) has been chosen as the bridging or terminal ligands of the boron, in which the electron deficiency of boron has been significantly weakened by the B–X–B or X–B dative π bonds, enhancing the electronic stability of the boron-based ptC; simultaneously, the lone pair/lone pair repulsion between the B atoms has been eliminated by the strong B–X bonds, providing steric protection for the ptC.

Nitrogen, as the neighbor of carbon, generally has the same non-classical bonding preferences as carbon,[14] of which the most typical is probably the planar tetracoordinate nitrogen (ptN). Since 1970, some ptN global energy minima (GEM) have

[a] *Institute of Molecular Science, Shanxi University, Taiyuan, 030006, People's Republic of China. E-mail: 202012801006@email.sxu.edu.cn*
[b] *School of Chemistry and Chemical Engineering, Shanxi University, Taiyuan, 030006, People's Republic of China*

† Electronic supplementary information (ESI) available. See DOI: https://doi.org/10.1039/d3cp05290g

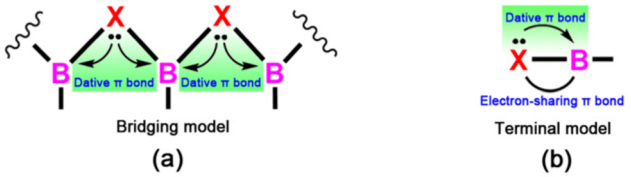

Scheme 1 The models of electron-compensation strategy proposed by Wu *et al.*

been successfully designed, such as NAl_4^-,[15] $NXAl_3^+$ (X = N, P and As),[16] and NAl_4Zn^+,[17] *etc.* Similarly, ptN-NM_4^+ (M = B, Al, Ga, In and Tl) is also of interest to theoretical chemists.[18] In 2023, Wu *et al.* designed ptN-$NAl_4S_4^+$ and found that it has an excellent stability.[19] But the ttN configuration was not mentioned in this study, because the GEM of NAl_4^+ adopts the planar tricoordinate nitrogen. Naturally, we noticed NGa_4^+, for which ptN-NGa_4^+ (**0d**) is electronically unstable and ttN-NGa_4^+ (**0a**) is the GEM, as shown in Fig. S1 (ESI†). Here, we wonder if the electron-compensation strategy can be used to stabilize the ptN but destabilize the ttN. To answer this question, we introduced four S atoms to ptN-NGa_4^+ and ttN-NGa_4^+, respectively. Satisfyingly, the ptN-$NGa_4S_4^+$ is more stable than the ttN-$NGa_4S_4^+$, electronically, thermodynamically and dynamically.

Computational methods

For ptN-$NGa_4S_4^+$ (**1a**), the geometry optimization and vibrational frequency calculations were performed at both the B3LYP/aug-cc-pVTZ and B2PLYP-D3(BJ)[20]/aug-cc-pVTZ levels; as expected, almost identical structures with similar imaginary frequencies were obtained at the two levels. In this test, we reported the geometric structure parameters calculated at the B2PLYP-D3(BJ)/aug-cc-pVTZ level. There are several available algorithms for searching potential energy surfaces (PESs), including the stochastic search algorithm,[21] ABC algorithm,[22] genetic algorithm,[23] PSO algorithm,[24] *etc.* The PES of $NGa_4S_4^+$ was explored using the stochastic search algorithm. Randomly generated structures were initially optimized at the B3LYP/6-31G(d) level, including both singlet and triplet surfaces. Then, the fifteen low-energy isomers were studied with further re-optimization and frequency calculation at the B2PLYP-D3(BJ)/aug-cc-pVTZ level. Finally, the first five lower isomers were selected and their energies were further refined by single-point calculations at the CCSD(T)/aug-cc-pVTZ level based on the B2PLYP-D3(BJ)/aug-cc-pVTZ optimized geometries. The relative energies of the isomers were determined by the sum of CCSD(T)/aug-cc-pVTZ energies and B2PLYP-D3(BJ)/aug-cc-pVTZ zero-point energy (ZPE) corrections. The dynamic stability was assessed by Born–Oppenheimer molecular dynamic (BOMD)[25] simulations at the PBE/DZVP level for 100 ps using the CP2K package.[26] The vertical detachment energies (VDEs) and vertical electron affinities (VEAs) were calculated at the OVGF/aug-cc-pVTZ level using the outer valence Green's function (OVGF) procedure.[27] The electronic structure of **1a** was deeply analyzed by the adaptive natural density partitioning (AdNDP)[28] analyses and the natural bond orbital (NBO)[29] at the B3LYP/6-31G(d) and B2PLYP-D3(BJ)/aug-cc-pVTZ levels, respectively. Simultaneously, the nucleus independent chemical shift (NICS) analyses[30] were performed at the B3LYP/aug-cc-pVTZ level. The stochastic search algorithm was performed using the GXYZ 2.0 program,[31] the AdNDP was analyzed using the AdNDP program,[32] the cross sections of NICS (CS-NICS) were generated with the Multiwfn 3.8 code,[33] the CCSD(T) calculations were carried out using the MolPro 2012.1 package,[34] and all other calculations were performed using the Gaussian 16 package.[35]

Structures designed

Exploring the electronic structure of ttN-NGa_4^+ (**0a**) might give us some clues about stabilizing ptN-NGa_4^+ (**0d**). AdNDP analyses of **0a** found that the $4s^2$ lone pair/$4s^2$ lone pair repulsion has forced the four Ga atoms away from each other to adopt the ttN configuration, as shown in Fig. S2 (ESI†). Hence, we first chose the electronegative O atom as the bridging ligand and designed ptN-$NGa_4O_4^+$, eliminating the lone pair/lone pair repulsion and electron deficiency of Ga. Unfortunately, the ptN-$NGa_4O_4^+$ has one imaginary frequency at 200i cm^{-1}. Then, the O atom was replaced by an S atom, as shown in Fig. 1, and ptN-$NGa_4S_4^+$ (**1a**) was the energy minimum with the smallest vibrational frequency at 18 cm^{-1}. The N–Ga interatomic distance is 1.937 Å in **1a**, which is in reasonable agreement with the bond length of the N–Ga single bond (2.087) in ttN-NGa_4^+ (**0a**), so **1a** is an eligible ptN species.

Stability consideration

The thermodynamic stability of **1a** was investigated by exploring its PESs using the stochastic search algorithm. The relative energies of the first five lower isomers were compared at the CCSD(T)/aug-cc-pVTZ level considering the zero-point energy (ZPE) corrections at the B2PLYP-D3(BJ)/aug-cc-pVTZ (abbreviated as CCSD(T) + $ZPE_{B2PLYP\text{-}D3(BJ)}$). As shown in Fig. 2, **1a** is the global energy minimum, displaying excellent thermodynamic stability. Notably, the isomer possessing ttN (**1c**) is a high-energy local minimum, which is 46.7 kcal mol^{-1} higher in energy than **1a**, indicating that the thermodynamic stability of ptN was significantly enhanced but that of ttN was weakened after introducing the four S atoms to NGa_4^+. It is proved that the electron-compensation strategy is suitable for stabilizing the ptN in this case.

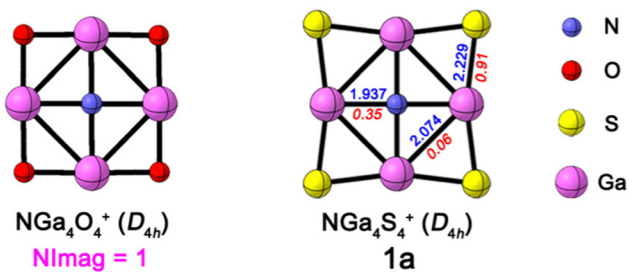

Fig. 1 Optimized structures of $NGa_4O_4^+$ and $NGa_4S_4^+$ (**1a**) regarding symmetry. Bond distances (in Å) and Wiberg bond orders are given in blue and italic red fonts, respectively.

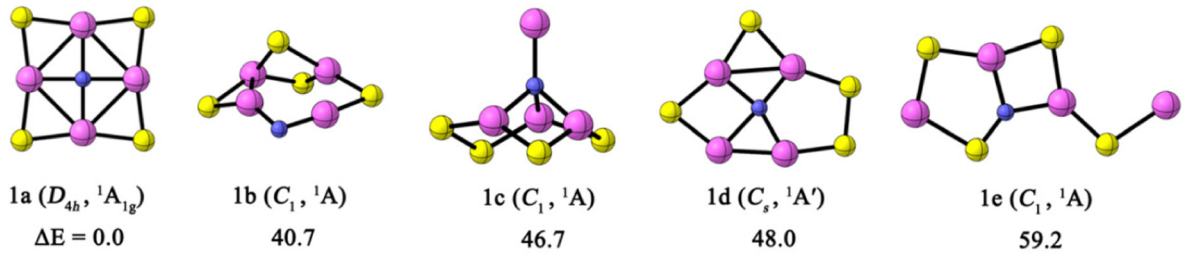

Fig. 2 Structures and relative energies (ΔE, in kcal mol^{-1} at the CCSD(T)+ZPE$_{B2PLYP\text{-}D3(BJ)}$ level) of **1a** and the low-energy isomers.

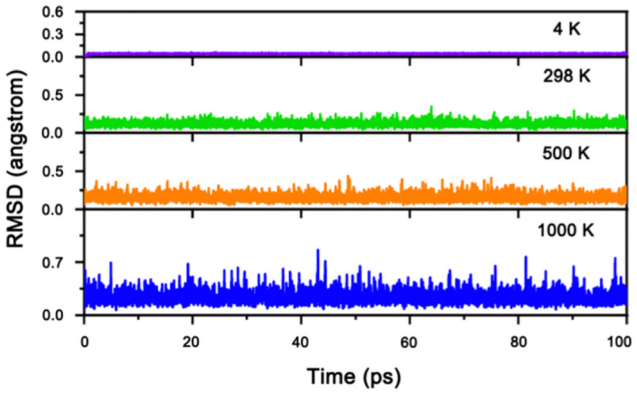

Fig. 3 The RMSD plots for the BOMD simulations of **1a** at 4 K, 298 K, 500 K and 1000 K, respectively.

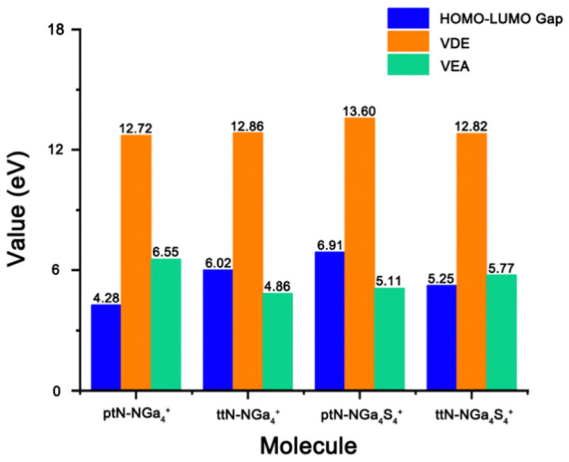

Fig. 4 The HOMO–LUMO gap values, VDEs and VEAs of ptN-NGa$_4^+$ (**0d**), ttN-NGa$_4^+$ (**0a**), ptN-NGa$_4$S$_4^+$ (**1a**), and ttN-NGa$_4$S$_4^+$ (**1c**).

The dynamic stability of **1a** was evaluated by performing the 100 ps BOMD simulations at 4, 298, 500 and 1000 K, respectively. The root-mean-square deviation (RMSD, in Å) plots describe structural evolution relative to the B2PLYP-D3(BJ)/aug-cc-pVTZ-optimized geometry during the simulations. Fig. 3 shows that **1a** had no irreversible upward jump at the PBE/DZVP level. Very small fluctuations of RMSD values were noted in the four simulations, specifically 0.01 to 0.06 Å for 4 K, 0.04 to 0.35 Å for 298 K, 0.06 to 0.44 Å for 500 K and 0.07 to 0.86 Å for 1000 K and with average RMSD values of 0.04, 0.12, 0.16 and 0.24 Å, respectively. The results of BOMD simulations indicated that **1a** is dynamically stable at the four considered temperatures and has properties against isomerization and dissociation. But, ttN-NGa$_4$S$_4^+$ (**1c**) is isomerized at 1000 K, as shown in Fig. S3 (ESI†). Hence, **1c** is dynamically viable.

Electronic structure analysis

We explored the factors that made **1a** stable from its electronic structure. As shown in Fig. 4, the introduction of four S atoms made the HOMO–LUMO gap of ptN species wider, specifically ptN-NGa$_4^+$ (**0d**, 4.28 eV) *versus* ptN-NGa$_4$S$_4^+$ (**1a**, 6.91 eV). Conversely, the value of ttN-NGa$_4^+$ (**0a**, 6.02 eV) is greater than that of ttN-NGa$_4$S$_4^+$ (**1c**, 5.25 eV). Besides, **1a** has a high VDE of 13.22 eV and low VEA of 5.11 eV at the OVGF/aug-cc-pVTZ level. So, **1a** is electronically stable showing a low trend to excite, lose and gain electrons. This indeed proves that the introduction of an S atom is beneficial for stabilization of ptN.

To further explore the electronic structure of **1a**, the AdNDP was analysed at the B3LYP/6-31G(d) level and the results are shown in Fig. 5. The peripheral bonding environment of **1a** included four 1c–2e S lone pairs (element **A**, ON = 1.96 |e|), eight 2c–2e Ga–S σ-bonds (element **B**, ON = 1.96 |e|) and four 3c–2e Ga-S-Ga π-bonds (element **C**, ON = 2.00 |e|). It was found that the eight less-diffuse Ga–S σ-bonds had eliminated the 4s^2 lone pair/4s^2 lone pair repulsion in **0a**, promoted the formation of the ptN and provided space protection for **1a**, which was consistent with the calculated Wiberg bond orders for Ga–S

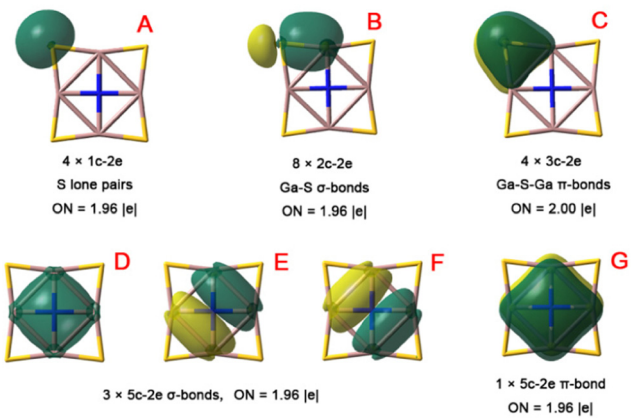

Fig. 5 AdNDP bonding patterns of **1a** with occupation numbers (ONs).

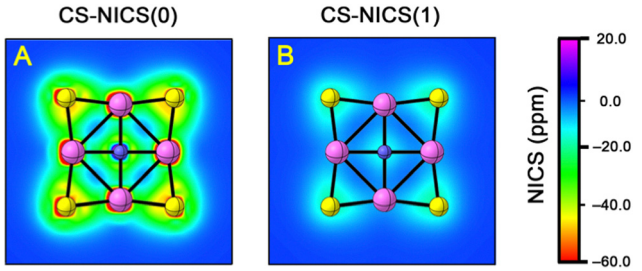

Fig. 6 NICS results for **1a**. Panels **A** and **B** correspond to the molecular planes and the planes parallel to and the plane of 1 Å above the molecular plane, respectively.

(0.91, see Fig. 1). According to the electron-compensation strategy, S atoms can compensate electrons for Ga atoms by the four π back-bonds, greatly reducing the electron-deficiency of Ga atoms and enhancing the stability of ptN. This can explain why **1a** is more stable than **1c**. Moreover, the four delocalized 5c–2e bonds may make a significant contribution to the thermodynamic and dynamic stability of **1a**, including three delocalized 5c–2e σ-bonds (elements **D**, **E** and **F**, ON = 1.96 |e|) and one delocalized 5c–2e π-bond (element **G**, ON = 1.96 |e|). The six σ and two π electrons meet the Hückel's $4n+2$ rule for n = 1 and 0, respectively. The σ and π double aromaticity further enhanced the stability of **1a**.

The nucleus-independent chemical shift (NICS) calculations were performed to verify the aromaticity of **1a**. Here, we just focus on the cross sections of NICS (CS-NICS) located at the molecular plane (CS-NICS(0)) and the plane of 1 Å above the molecular plane (CS-NICS(1)), respectively. Fig. 6 shows the color-filled maps of CS-NICS(0) and CS-NICS(1). From the color distribution of Fig. 6A, the colors representing the negative NICS values have filled almost the entire region of the molecule, demonstrating the existence of strong aromaticity in the molecular plane, while the light blue region within the NGa_4 moiety in the CS-NICS(1) plot (Fig. 6B) indicates the slightly weak aromatic electron circulations in the plane of 1 Å above the molecular plane. Therefore, **1a** is aromatic, consistent with the AdNDP analysis.

Conclusions

In summary, we have computationally demonstrated the applicability of an electron-compensation strategy in designing a ptN species, $NGa_4S_4^+$. The results showed that the introduction of four electronegative S atoms greatly enhanced the stability of ptN but weakened ttN, electronically, thermodynamically and dynamically. The four S atoms eliminated the lone pair/lone pair repulsion by the eight 2c–2e Ga–S σ bonds and reduced the electron deficiency of Ga by four 3c–2e Ga–S–Ga π back-bonds. In addition, the σ and π double aromaticity makes **1a** more stable. Therefore, as the dynamically stable global energy minimum displays double 6σ/2π aromaticity, ptN-$NGa_4S_4^+$ is more likely to be detected in the gas phase than ttN-$NGa_4S_4^+$.

Conflicts of interest

There are no conflicts to declare.

Acknowledgements

The authors would like to thank Professor Yan-bo Wu of Shanxi University for the support and guidance during this work, as well as the HPC of Shanxi University for the support.

Notes and references

1 L.-M. Yang, E. Ganz, Z. Chen, Z.-X. Wang and P. V. R. Schleyer, *Angew. Chem., Int. Ed.*, 2015, (54), 9468–9501.
2 R. Hoffmann, R. W. Alder and C. F. Wilcox, *J. Am. Chem. Soc.*, 1970, **92**, 4992–4993.
3 J. H. van't Hoff, *Arch. Neerl. Sci. Exactes Nat.*, 1874, **9**, 44.
4 J. A. Le Bel, *Bull. Soc. Chim. Fr.*, 1874, **22**, 337.
5 X. Li, H.-f Zhang, L.-S. Wang, G. D. Geske and A. I. Boldyrev, *Angew. Chem., Int. Ed.*, 2000, **39**, 3630–3632.
6 X. Li, L.-S. Wang, A. I. Boldyrev and J. Simons, *J. Am. Chem. Soc.*, 1999, **121**, 6033–6038.
7 A. I. Boldyrev and L.-S. Wang, *J. Phys. Chem. A*, 2001, **105**, 10759–10775.
8 (*a*) Y.-B. Wu, J.-L. Jiang, H. Li, Z. Chen and Z.-X. Wang, *Phys. Chem. Chem. Phys.*, 2010, **12**, 58–61; (*b*) F. Dong, S. Heinbuch, Y. Xie, J. J. Roccab and E. R. Bernstein, *Phys. Chem. Chem. Phys.*, 2010, **12**, 2569–2581.
9 (*a*) Y.-B. Wu, J.-L. Jiang, H.-G. Lu, Z.-X. Wang, N. Perez-Peralta, R. Islas, M. Contreras, G. Merino, J. I-Chia Wu and P. V. R. Schleyer, *Chem. – Eur. J.*, 2011, **17**, 714–719; (*b*) C.-J. Zhang, P. Wang, X.-L. Xu, H.-G. Xu and W.-J. Zheng, *Phys. Chem. Chem. Phys.*, 2021, **23**, 1967–1975.
10 V. Vassilev-Galindo, S. Pan, K. J. Donald and G. Merino, *Nat. Rev. Chem.*, 2018, **2**, 0114.
11 L. Leyva-Parra, L. Diego, O. YaÇez, D. Inostroza, J. Barroso, A. Vásquez-Espinal, G. Merino and W. Tiznado, *Angew. Chem., Int. Ed.*, 2021, **60**, 8700–8704.
12 Z. X. Wang and P. V. R. Schleyer, *J. Am. Chem. Soc.*, 2001, **123**, 994–995.
13 B. Jin, C. Yuan, G. Lu and Y.-B. Wu, *Chem. Commun.*, 2022, **58**, 1309–13098.
14 (*a*) S.-D. Li, G.-M. Ren, C.-Q. Miao and Z.-H. Jin, *Angew. Chem., Int. Ed.*, 2004, **43**, 1371–1373; (*b*) S.-D. Li, C.-Q. Miao and G.-M. Ren, *Eur. J. Inorg. Chem.*, 2004, 2232–2234.
15 S. K. Nayak, B. K. Rao, P. Jena, X. Li and L. S. Wang, *Chem. Phys. Lett.*, 1999, **301**, 379–384.
16 Z.-h Cui and Y.-h Ding, *Phys. Chem. Chem. Phys.*, 2011, **13**, 5960–5966.
17 X.-d Jia and Z.-w Du, *Phys. Chem. Chem. Phys.*, 2023, **25**, 4211–4215.
18 (*a*) X. Li and L. S. Wang, *Eur. Phys. J. D*, 2005, **34**, 9–14; (*b*) B. B. Averkiev, A. I. Boldyrev, X. Li and L.-S. Wang, *J. Chem. Phys*, 2006, **125**, 124305; (*c*) B. Song, C.-H. Yao and P.-L. Cao, *Phys. Rev. B: Condens. Matter Mater. Phys.*, 2006, **74**, 035306; (*d*) B. B. Averkiev, A. I. Boldyrev, X. Li and

L.-S. Wang, *J. Phys. Chem. A*, 2007, **111**, 34–41; (*e*) B. B. Averkiev, S. Call, A. I. Boldyrev, L.-M. Wang, W. Huang and L.-S. Wang, *J. Phys. Chem. A*, 2008, **112**, 1873–1879; (*f*) W.-Q. Zhang, J.-M. Sun, G.-F. Zhao and L.-L. Zhi, *J. Chem. Phys*, 2008, **129**, 064310; (*g*) L.-M. Wang, W. Huang, L.-S. Wang, B. B. Averkiev and A. I. Boldyrev, *J. Chem. Phys.*, 2009, **130**, 134303; (*h*) H. Wang, Y. J. Ko, K. H. Bowen, A. P. Sergeeva, B. B. Averkiev and A. I. Boldyrev, *J. Phys. Chem. A*, 2010, **114**, 11070–11077.

19 R. Sun, C. Yuan, H.-J. Zhai and Y.-B. Wu, *J. Chem. Phys.*, 2023, **158**, 144301.

20 S. Grimme, S. Ehrlich and L. Goerigk, *J. Comput. Chem.*, 2011, **32**, 1456–1465.

21 (*a*) M. Saunders, *J. Comput. Chem.*, 2004, **25**, 621–626; (*b*) P. P. Bera, K. W. Sattelmeyer, M. Saunders, H. F. Schaefer and P. V. R. Schleyer, *J. Phys. Chem. A*, 2006, **110**, 4287–4290.

22 J. Zhang and M. Dolg, *Phys. Chem. Chem. Phys.*, 2015, **17**, 24173–24181.

23 O. Yañez, R. Báez-Grez, D. Inostroza, W. A. Rabanal-León, R. Pino-Rios, J. Garza and W. Tiznado, *J. Chem. Theory. Comput.*, 2019, **15**, 1463–1475.

24 Y. Wang, J. Lv, L. Zhu and Y. Ma, *Comput. Phys. Commun.*, 2012, **183**, 2063–2070.

25 (*a*) J. M. Millam, V. Bakken, W. Chen, W. L. Hase and H. B. Schlegel, *J. Chem. Phys.*, 1999, **111**, 3800–3805; (*b*) X. S. Li, J. M. Millam and H. B. Schlegel, *J. Chem. Phys.*, 2000, **113**, 10062–10067.

26 T. D. Kühne, *et al.*, *J. Chem. Phys.*, 2020, **152**, 194103.

27 J. V. Ortiz, V. G. Zakrzewski and O. Dolgounircheva, *Conceptual Perspectives in Quantum Chemistry*, Kluwer Academic, 1997.

28 D. Y. Zubarev and A. I. Boldyrev, *Phys. Chem. Chem. Phys.*, 2008, **10**, 5207–5217.

29 A. E. Reed, L. A. Curtiss and F. Weinhold, *Chem. Rev.*, 1988, **88**, 899–926.

30 (*a*) P. V. R. Schleyer, C. Maerker, A. Dransfeld, H. J. Jiao and N. Hommes, *J. Am. Chem. Soc.*, 1996, (118), 6317–6318; (*b*) Z. Chen, C. S. Wannere, C. Corminboeuf, R. Puchta and P. V. R. Schleyer, *Chem. Rev.*, 2005, **105**, 3842–3888.

31 (*a*) Y.-B. Wu, H.-G. Lu, S.-D. Li and Z.-X. Wang, *J. Phys. Chem. A*, 2009, **113**, 3395–3402; (*b*) H. G. Lu and Y. B. Wu, *GXYZ2.0, A Random Search Program*, Shanxi University, Taiyuan, 2015.

32 The AdNDP program was downloaded freely at, **https://ion.chem.usu.edu/~boldyrev/adndp.php**.

33 T. Lu and F. W. Chen, *J. Comput. Chem.*, 2012, **33**, 580–592.

34 H.-J. Werner, *et al.*, *MolPro.2012.1*, University College Cardiff Consultants Limited, Cardiff, U.K., 2012.

35 M. J. Frisch, *et al. Gaussian 16 Revision A.03*, Gaussian Inc., 2016.